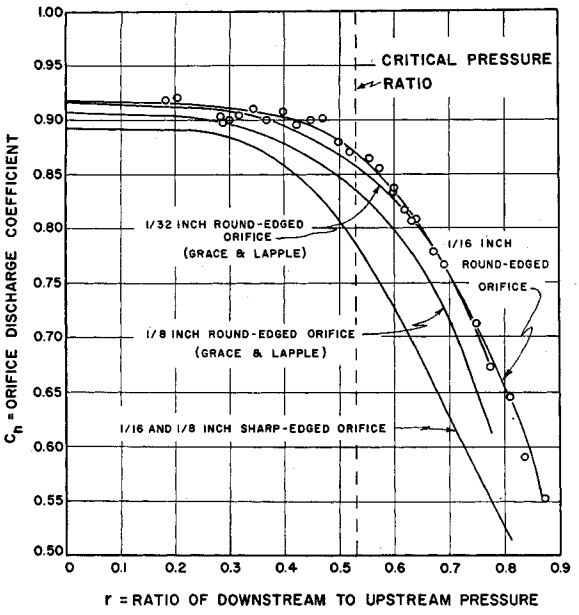

Fig. 7. Round-edged orifice.

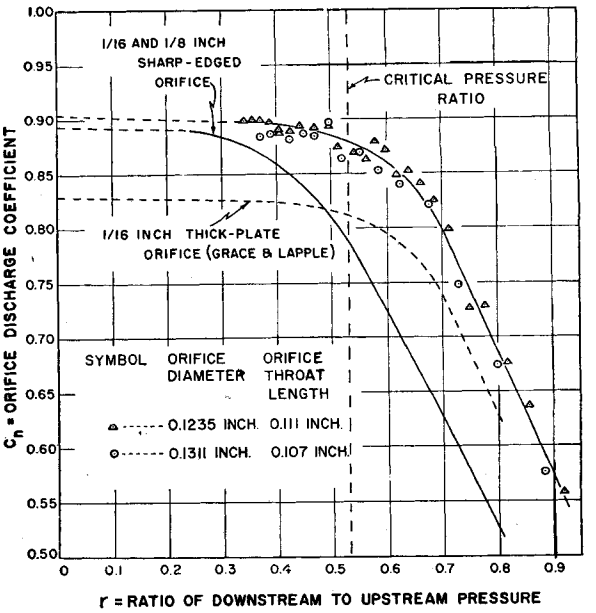

Fig. 8. Thick-plate orifice.

than 0.33. Inasmuch as bubble formation occurring close to the downstream face of a sharp-edged orifice operating in the air-water system influences the effective orifice discharge area, liquid physical properties may be expected to be important in determining the rate of flow from this type of orifice for other gas-liquid systems. Before a generalized correlation can be developed for the flow of gases into liquids through single submerged orifices further data must be obtained for systems containing liquids other than water.

NOTATION

		Dimension
A_o	= orifice cross-sectional area	L^2
C_n	= orifice coefficient of discharge	
D_o	= orifice diameter	L
g_c	= conversion factor = 32.17 (lb./lb. force)(ft./sec.^{2})	$ML/F\theta^2$
k	= ratio of specific heat at constant pressure to specific heat at constant volume	
L_o	= orifice throat length	
M_W	= molecular weight, lb./lb. mole	
P_1	= absolute pressure upstream from the orifice	F/L^2
P_2	= absolute pressure downstream from the orifice	F/L^2
q	= volumetric rate of air flow at standard conditions, 32°F. and 14.7 lb. force/sq. in.	L^3/θ
R	= gas constant	LF/MT
r	= ratio of absolute pressure downstream from the orifice to the absolute pressure upstream from the orifice	
T_1	= absolute temperature upstream from the orifice	T
T_2	= temperature of the air flowing from the experimental column	T
w	= mass flow rate	M/θ
β	= ratio of orifice diameter to orifice-assembly-tube diameter	
ρ_1	= gas density upstream from the orifice	M/L^3

LITERATURE CITED

1. Achorn, G. B., and J. L. Schwab, *Science*, **107**, 377 (1948).
2. Am. Soc. Mech. Engrs., "Fluid Meters —Their Theory and Application," New York (1951).
3. Blackshear, P. L., *Trans. Am. Soc. Mech. Engrs.*, **75**, 51 (1953).
4. Cox, G. N., and F. J. Germano, "Fluid Mechanics," D. Van Nostrand Company, New York (1941).
5. Cunningham, R. G., *Trans. Am. Soc. Mech. Engrs.*, **73**, 625 (1951).
6. Datta, R. L., D. H. Napier, and D. M. Newitt, *Trans. Inst. Chem. Engrs.*, **28**, 14 (1950).
7. Davidson, L., Ph.D. thesis, Columbia Univ., New York (1951).
8. Dodge, B. F., "Chemical Engineering Thermodynamics," p. 331, McGraw-Hill Book Company, Inc., New York (1944).
9. Dzienisiewicz, J., Ph.D. thesis, Royal School of Mines, Univ. London (1951).
10. Eversole, W. G., G. H. Wagner, and E. Stackhouse, *Ind. Eng. Chem.*, **33**, 1459 (1941).
11. Fischer, F., and K. Peters, *Ges. Abhandl. Kenntnis Kohle*, 11, 441 (1934).
12. Grace, H. P., and C. E. Lapple, *Trans. Am. Soc. Mech. Engrs.*, **73**, 639 (1951).
13. Hartshorn, L., *Proc. Roy. Soc. (London)*, **A94**, 155 (1918).
14. Hughes, R. R., A. E. Handlos, H. D. Evans, and R. L. Maycock, paper presented at San Francisco meeting, Am. Inst. Chem. Engrs. (Sept. 14, 1953).
15. Maier, G. G., *U. S. Bur. Mines Bull.* 260, 62 (1927).
16. Pattle, R. E., *Trans. Inst. Chem. Engrs.*, **28**, 32 (1950).
17. Perry, J. A., *Trans. Am. Soc. Mech. Engrs.*, **71**, 757 (1949).
18. Prandtl, L., "Essentials of Fluid Mechanics," Hafner Publishing Company, New York (1952).
19. Reynolds, H., *Trans. Am. Soc. Mech. Engrs.*, **38**, 799 (1916).
20. Schiller, W., *Forsch. Gebiete Ingenieurw.*, **4**, 128 (1933).
21. Spells, K. E., and S. Bakowski, *Trans. Inst. Chem. Engrs.*, **28**, 38 (1950).
22. *Ibid.*, **30**, 189 (1952).
23. Stanton, T., *Proc. Roy. Soc. (London)*, **A111**, 306 (1926).
24. Van Krevelen, D. W., and P. J. Hoftijzer, *Chem. Eng. Progr.*, **46**, 29 (1950).

II. Mechanics of Bubble Formation

Very little information is available concerning bubble formation and behavior at the high rates of gas flow reported in Part 1. The purpose of this paper is to develop an understanding of the mechanics of formation and detachment of bubbles from single, submerged orifices operating at relatively high rates of air flow in a high-seal liquid-level system. Studies of these phenomena by use of orifices, nozzles, capillaries, and porous plates operating at low rates of gas flow have been made by many investigators (*5, 8, 9, 15, 28*) and were thoroughly reviewed by Jackson (*16*).

PREVIOUS WORK

Studies of bubble formation reported in the literature show that as the rate of gas flow through the orifice is increased, three regions of bubble formation are obtained. At very low rates of gas flow (below the

range covered in this paper) bubble formation is a static problem, bubble size being determined primarily by orifice diameter, surface tension, and fluid densities. In fact, the basis of the drop-volume (*13*) method of measuring surface tension is the formation of bubbles from fine capillaries at practically zero rate of gas flow. At low rates of gas flow previous work (*1, 7, 8*) has shown that for any given system and orifice diameter, bubble size is constant with respect to gas-flow rate. At intermediate rates of gas flow bubbles are formed at a constant frequency and the bubble size is uniform and depends primarily on the rate of gas flow, the orifice diameter, and the volume of the gas chamber upstream from the orifice. Van Krevelen and Hoftijzer (*29*) on the basis of studies using capillaries less than 0.02 in. in diameter claim that bubble size is independent of capillary-tip diameter. However, Davidson (*8*) shows that bubble size is approximately proportional to the square root of the orifice diameter for bubble formation at constant frequency. The effect of liquid physical properties such as surface tension, viscosity, and density is not clear (*12, 24*). Some authors (*5, 7, 11, 16, 21, 26, 29, 30*) have observed the formation of clouds of minute bubbles upon the addition to water of small amounts of acetic acid, alcohols, or surface-active agents. Davidson (*8*) showed that an increase in liquid viscosity tends to cause an increase in bubble size. At high rates of gas flow, the bubbles formed are not uniform in size and no data have been found in the literature to show the effects of rate of gas flow or orifice diameter on the bubble-size distribution.

APPARATUS

The experimental equipment used for this study was described in Part I. A Kodak 16-mm. high-speed motion picture camera, equipped with a Kodak Cine Ektar 63-mm. f/2 lens, was used to obtain motion pictures of the bubble formation. At full voltage of 115 volts this machine has a top film speed of 3,000 frames/sec. Illumination was provided by five G. E. 750-watt intermittent lamps. The number and position of these lamps were determined by trial and error. The optimum conditions were found to be two top lights (front and back), one center light (front), and two bottom lights (front and back). Kodak Super XX high-speed panchromatic reversal film type III, Class L-1, was used. The sharpest definition of the small bubbles was obtained by use of a black background.

Several hundred photographs of the bubbles were taken, both at the orifice and at a section approximately 3 ft. above the level of the orifice. A 4- by 5-in. Speed Graphic camera, equipped with a Kodak Ektar 127-mm. f/4.7 lens and Super panchromatic press type B film, was used. Lighting was provided by a No. 1 Strobonar Heiland Model HR3 lamp flashing for 1/2,000 sec. This lamp was held above the camera by hand and canted at a 45-deg. angle to the column. The distance from the focal plane of the camera to the column varied between 1 and 2 ft. The maximum depth of field was obtained with a lens aperture of f/22 with the camera focused on the center line of the column.

At intermediate rates of air flow, stroboscopic studies were performed to determine the frequency of bubble formation with a General Radio Company strobotac. Observations of bubble formation were limited to bubbles in the immediate proximity of the orifice. With the onset of turbulence in the air stream flowing through the orifice, shifting frequencies of formation were obtained and in some cases visibility was greatly reduced by the clouds of very small bubbles which were formed. Under these conditions the accurate determination of the frequency of bubble formation is also seriously handicapped by the surface irregularities in the bubbles of the air stream emerging from the orifice. The reproducibility of results was enhanced by attempting to "stop" the motion of the bubble forming at the orifice.

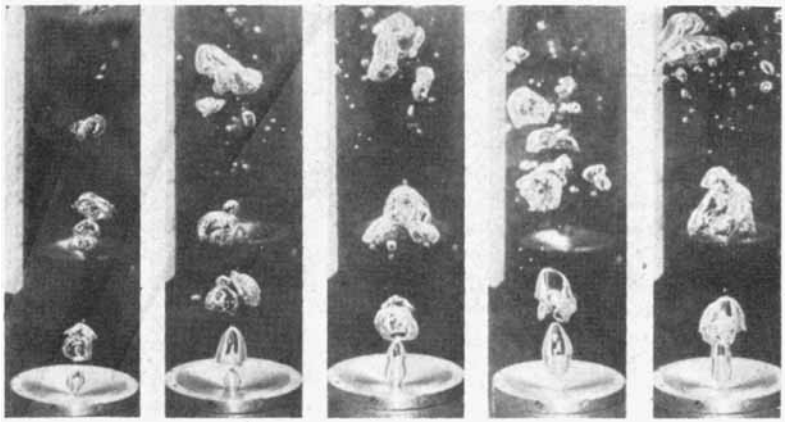

Fig. 1 through 5. Flow of air into water through 1/16-in. orifice; (1) $N_{Re} = 700$, (2) $N_{Re} = 1{,}088$, (3) $N_{Re} = 1{,}800$, (4) $N_{Re} = 2{,}050$, (5) $N_{Re} = 2{,}250$.

DESCRIPTION OF BUBBLE BEHAVIOR

To understand the mechanics of bubble formation at high rates of gas flow, a review of the mechanism of formation and detachment of bubbles at low flow rates is desirable. As a bubble forms, the surrounding liquid is accelerated away from the opening by viscous drag forces acting on the top surface of the bubble. If the volume of the gas chamber upstream from the orifice is small, the chamber pressure drops slightly because of this liquid motion, and the growth of the bubble is decelerated. Since the rate of gas flow to the chamber is steady, the pressure rises again and the growth of the bubble is accelerated. As liquid circulates inward at the level of the opening, the bubble is necked in and detached by a combination of buoyant forces and the motion of the liquid toward the opening. The detached bubble rises and the portion of its volume remaining at the orifice becomes the nucleus of the next bubble to form.

Turner (*28*) states that during bubble formation at low flow rates no significant cyclical pressure fluctuations occur in the gas chamber below the orifice if the chamber volume is greater than 10^4 times the volume of an individual bubble issuing from the orifice. Bubble formation then becomes dependent on dynamic effects in the liquid and in the gas but is surprisingly little different in the absence of the pressure surges described. Other investigators (*15*) clearly demonstrate the importance of the gas-chamber volume below the orifice as a factor influencing bubble formation and point out that if the chamber volume is much greater than $(A_o\rho_o c^2/g_c\Delta\rho)$ the chamber pressure is constant. Both these conditions are met throughout most of the range in the present investigation and the results obtained should be applicable to large-scale equipment.

Early in the present study it was realized that most of the phenomena occurring at very high air-flow rates (with the orifice operating near the critical pressure ratio) might be explained by a study of the effect of gas turbulence and liquid circulation on bubble formation at lower rates of gas flow. Previous investigators (*15, 19*) have suggested that the formation of bubbles nonuniform in size as they pass through the orifice may be closely connected with gas turbulence. Figures 1 through 9 are a series of photographs showing bubble formation in water from a 1/16-in. sharp-edged orifice at Reynolds numbers (for gas flow through the orifice) varying from approximately 700 to 10,450. The photographs shown in Figures 1 through 4 reveal that bubbles relatively uniform in size are produced for laminar flow of air through the orifice (i.e., at Reynolds numbers less than 2,100). In this range as a bubble is detached from the orifice some very small bubbles are formed by the rupture and collapse of the elongated bubble neck. This is illustrated in Figure 4 by the small bubble shown between the large detached bubble and the growing bubble at the orifice. In Figures 1 through 4 small bubbles are present between the large bubbles near the orifice. Thus in the laminar-flow range bubbles much smaller than the average bubble size may be formed by the rupture and collapse of the elongated bubble neck as liquid circulates inward at the level of the orifice.

As the flow rate is increased (Figures 1 to 4), the bubble formed at the orifice

changes from a smooth sharply defined ellipsoid (Figure 1) to a pear-shaped bubble (Figure 2), which becomes increasingly elongated at higher flow rates (Figures 3 and 4). Incipient coalescence, a condition in which one bubble is projected into, and may become totally enclosed by, the one immediately above, is shown by the second bubble above the orifice in Figures 3 and 4. In the laminar-flow range, high-speed motion pictures show that upon detachment the bubble is swept by a surface wave which initiates at the bottom of the bubble and films over the entire bubble with fresh liquid. At the conclusion of the surface wave the bubble appears to be helmet shaped with a flat bottom (Figure 2). Jakob and Fritz (*17*) have photographed bubbles of this shape near heat transfer surfaces during their study of bubble formation in boiling liquids. Yamagata (*32*) et al. have observed that single steam bubbles (both spherical and helmet shaped) are formed in boiling water in the free-convection region. In the forced-convection region steam-bubble formation was found to be a function of the degree of turbulence in the boundary layer near the heat transfer surface, and nonuniform steam bubbles were produced in this region of operation.

With the onset of turbulence for the gas flow through the orifice (Figures 5 through 9 for Reynolds numbers greater than 2,100), coalescence occurs very close to the orifice and the resultant large irregular bubble rises only a very small distance (3 to 4 in. above the opening) before it is shattered into many small bubbles of varying sizes. Many very small bubbles formed by this process are evident at a Reynolds number of 4,600 (Figure 8). As the Reynolds number increases to 10,000, the bubbles formed by the shattering process become smaller.

As gas turbulence becomes fully developed ($N_{Re} > 10{,}000$), stroboscopic examination and high-speed motion pictures show that what appears to the unaided eye to be a continuous jet of gas is actually a series of closely spaced, irregular bubbles rising with a very rapid counterclockwise swirling motion. A large number of very fine bubbles (Figure 9) are formed by being torn from the swirling air stream in a manner similar to that described for liquid sprays by Castelman (*2, 3*). Rough portions of the air-bubble surface (Figure 9) are pinched or torn off to form very minute bubbles. The formation of bubbles nonuniform in size is greatly accelerated by the virtual explosion of the large irregular bubbles at a point approximately 4 in. above the orifice. The jet of gas leaving the orifice is similar to a tornado or a waterspout. A combined vortex is formed composed of a forced vortex on an axis perpendicular to the plane of the orifice and a free vortex in the bulk of the liquid. Liquid circulates in a large eddy near the orifice, flowing toward the jet at the level of the orifice, rotating very rapidly around the central core of bubbles, and flowing away from the top of the forced vortex as gas-liquid mixing with the shattering of the large bubbles occurs. A series of photographs of bubble formation from orifices of other diameters corroborates the observations of bubble formation from the 1/16-in. sharp-edged orifice. Figures 10, 11, 12, and 13 for bubble formation from the 1/64-in. sharp-edged orifice submerged in water trace the development of turbulence in the air stream as the Reynolds number is increased from 621 to 9,470. Figure 10 shows that the bubbles produced for laminar flow of air through the 1/64-in. orifice are much smaller than those produced from the 1/16-in. orifice at a similar Reynolds number (Figure 1). As in Figure 1, the bubble forming at the orifice is a smooth, sharply defined ellipsoid. Figure 11 shows the bubble formation at a Reynolds number of 2,010. Some very small bubbles are apparent, and incipient coalescence occurs near the orifice. Figures 10 and 11 corroborate the relative

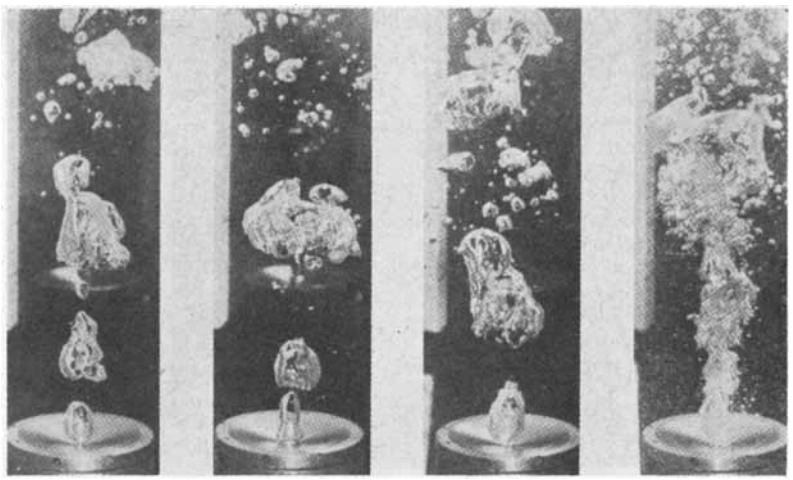

(6) (7) (8) (9)

Fig. 6 through 9. Flow of air into water through 1/16-in. orifice; (6) N_{Re} = 2,700, (7) N_{Re} = 3,680, (8) N_{Re} = 4,660, (9) N_{Re} = 10,450.

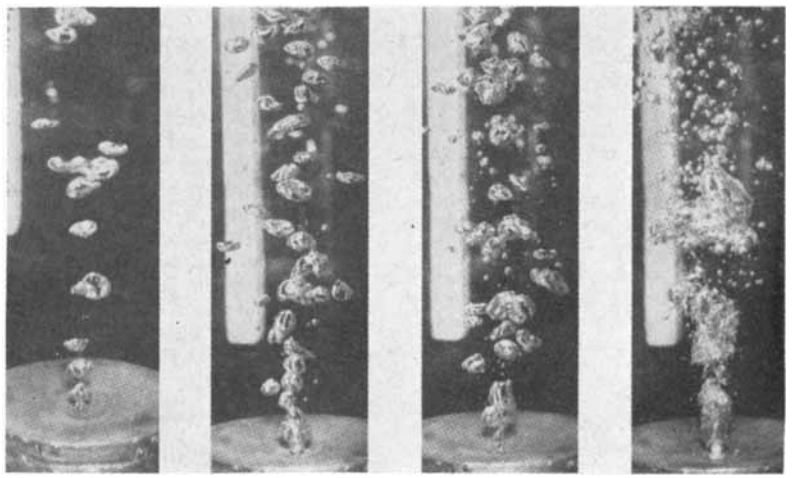

(10) (11) (12) (13)

Fig. 10 through 13. Flow of air into water through 1/64-in. orifice; (10) N_{Re} = 621, (11) N_{Re} = 2,010, (12) N_{Re} = 2,520, (13) N_{Re} = 9,470.

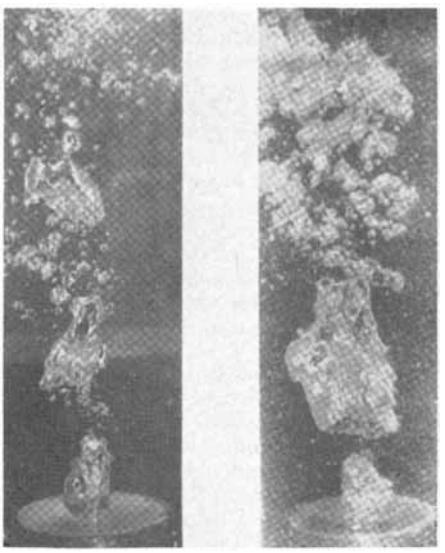

(14) (15)

Fig. 14 and 15. Flow of air into water: (14) N_{Re} = 7,760, 1/32-in. orifice; (15) N_{Re} = 9,460, 1/8-in. orifice.

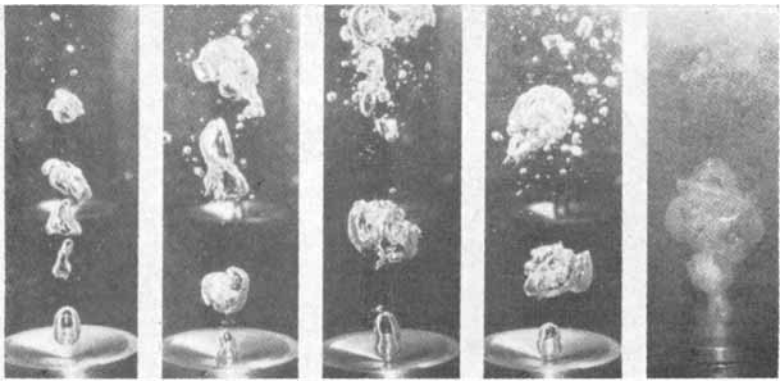

(16) (17) (18) (19) (20)

Fig. 16 through 20. Flow of air into 1.6% butanol solution through 1/16-in. orifice; (16) N_{Re} = 730, (17) N_{Re} = 1,780, (18) N_{Re} = 2,000, (19) N_{Re} = 2,310, (20) N_{Re} = 8,550.

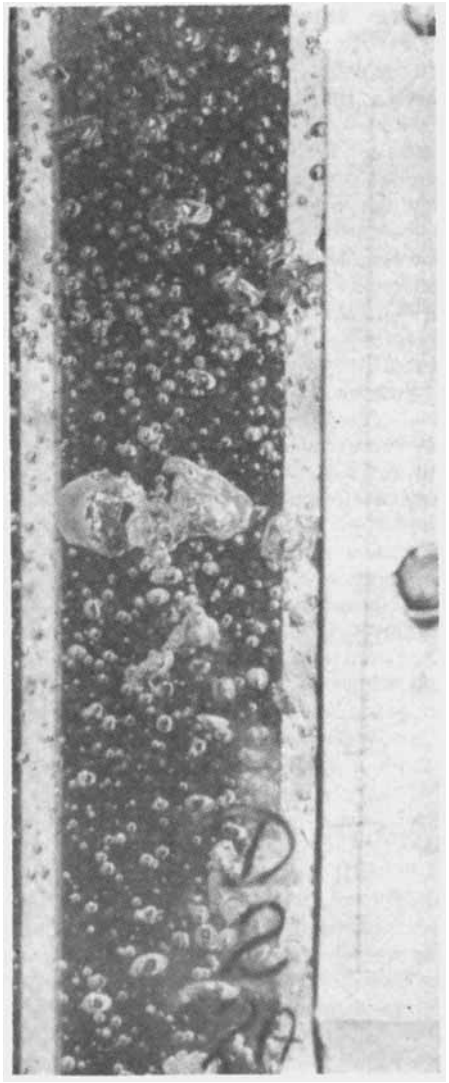

Fig. 21. 1/64-in. orifice; N_{Re} = 14,000, D_{vs} = 0.187.

uniformity of bubble size (shown by Figures 1 through 4) for the laminar flow of air through the orifice. Figure 12 shows the nonuniformity of bubble size characteristic of the onset of turbulent flow through the orifice. The mechanics of bubble formation for fully developed turbulence as shown in Figures 13, 14, and 15 for the 1/64-, 1/32-, and ⅛-in. orifices, respectively, are very similar to the bubble formation from the 1/16-in. orifice at a similar Reynolds number (Figure 9).

Several observations made from the high-speed motion pictures taken at high rates of gas flow through each of the orifices are of interest. At a Reynolds number of 20,000 many very small bubbles (smaller than 0.05 in. in diameter) are formed by being torn off the large swirling bubbles in the discontinuous jet. These fine bubbles rise with a relatively slow counterclockwise rotation about the discontinuous jet. Near the walls of the column the downward motion of the very small bubbles is indicative of liquid currents in the free vortex in the bulk of the liquid. Breakup of most of the large bubbles in the jet occurs approximately 3 to 4 in. above the orifice. At a Reynolds number of 30,000 the spiraling motion of the jet appears to be compressed and an intensified cloud of fine bubbles is present. For the orifice sizes larger than 1/64 in. a ring of fine bubbles appears very close to the orifice. These bubbles hang suspended with some motion of very small amplitude to and from the orifice. It is likely that the velocity of rise of the small bubbles near the orifice is of the same magnitude as the point velocity of the liquid circulating toward the orifice. Therefore the small bubbles of the ring are virtually trapped and can escape only when irregularities of flow occur. No ring of fine bubbles surrounding the orifice was observed for the 1/64-in. orifice until higher Reynolds numbers were reached. No marked changes in the flow regime were noted for any of the orifices as the pressure ratio decreased below 0.53 (the critical pressure ratio for air). The rapidly moving jet of bubbles appeared to be intermittently continuous in the motion pictures, an impression that stroboscopic examination of this jet suggests is a result of the superposition of discrete bubbles in different vertical and horizontal planes upon each other in such a manner that they overlap, giving the jet an appearance of continuity. At a Reynolds number of 40,000 the spiraling motion of the jet seemed to be compressed to an even greater extent. As the Reynolds number was increased, somewhat greater numbers of very small bubbles were formed by being torn off the very rapidly swirling core of large bubbles. At the greatest flow rates invesgitated, the visibility of phenomena at the orifice was very poor, inasmuch as the cloud of very fine bubbles formed rendered the liquid translucent.

Most of the phenomena described for bubble formation in the air-water system also occur for the formation of air bubbles in a 1.6% solution of butanol in water with a solution surface tension of 44.5 dynes/cm. Figures 16 through 20 are a series of photographs showing bubble formation from a 1/16-in. sharp-edged orifice submerged in an aqueous butanol solution for Reynolds numbers (for gas flow through the orifice) varying from approximately 730 to 8,550. Figures 16, 17, and 18 illustrate bubble behavior in the aqueous butanol solution in the laminar-flow range at approximately the same Reynolds numbers as Figures 1, 3, and 4, respectively. The most marked difference is the great increase in the number of very small bubbles formed in the butanol solution as the rate of air flow is increased. Figures 17 and 18 show several very small bubbles just above the bubble growing at the orifice. High-speed motion pictures and stroboscopic studies reveal that these small bubbles are produced by the collapse and rupture of the elongated bubble neck upon the detachment of a bubble from the orifice. Because of the low surface tension of the butanol solution, a larger number of small bubbles are formed in the butanol solution than in water at corresponding rates of air flow. Figure 19 shows the formation of bubbles nonuniform in size, resulting from the shattering of the rising bubble at a point approximately 4 in. above the orifice. As in Figure 5 (for water), the formation of bubbles of nonuniform size in the butanol solution is initiated with the onset of turbulence for the flow of the gas through the orifice. A comparison of Figures 19 and 5 shows that a much greater number of fine bubbles are formed in the butanol solution than in water. As the rate of air flow increases (Figure 20), a cloud of fine bubbles is formed which makes further observations difficult. However, stroboscopic examination reveals that as turbulence is fully developed for the air flow through the orifice, a counterclockwise spiraling, swirling motion of the air jet is initiated. Thus the major effect of lowering the surface tension of the seal liquid appears to be an increase in the formation of very small bubbles by a reduction in the amount of energy required to form a unit of interfacial area. The mechanisms by which very small bubbles are formed seem to be unaffected by changes in the surface tension of the seal liquid.

In summary, observation of bubble

TABLE 1. LAMINAR-FLOW RANGE

Point	Pressure ratio r	Flow rate q, cu. ft./min.	Reynolds number N_{Re}	Frequency f, bubbles/min.	Bubble diameter D_B, in.
Series B-15	Orifice diameter, D_0 = 0.0165 in. air-water system				
1	0.990	0.0061	630	1,110	0.275
2	0.983	0.0097	1,000	1,180	0.309
3	0.958	0.0161	1,660	1,200	0.364
4	0.952	0.0181	1,870	1,250	0.374
5	0.944	0.0197	2,030	1,300	0.379
Series B-17B	Orifice diameter, D_0 = 0.0165 in. air–aqueous butanol system				
1	0.994	0.0061	629	1,200	0.264
2	0.983	0.0102	1,050	1,270	0.308
3	0.965	0.0156	1,610	1,400	0.343
4	0.955	0.0177	1,820	1,350	0.362
5	0.948	0.0202	2,080	1,370	0.376
Series D-23	Orifice diameter, D_0 = 0.0635 in. air-water system				
1	0.996	0.0270	724	900	0.478
2	0.992	0.0415	1,110	1,000	0.532
3	0.989	0.0668	1,790	1,050	0.614
4	0.987	0.0759	2,030	1,050	0.614
Series D-24B	Orifice diameter, D_0 = 0.0635 in. air–aqueous butanol system				
1	0.996	0.0278	751	850	0.493
2	0.993	0.0393	1,040	920	0.535
3	0.989	0.0668	1,770	1,035	0.617
4	0.987	0.0758	2,040	1,040	0.642
Series A-17	Orifice diameter, D_0 = 0.1265 in. air-water system				
1	0.999	0.0234	314	650	0.507
2	0.980	0.0804	1,080	720	0.739
5	1.00	0.0048	64.2	202	0.440
6	0.999	0.0299	402	558	0.578
7	0.999	0.0294	395	795	0.511
8	0.984	0.0421	566	740	0.590

formation over a wide range of rates of air flow indicates that very small bubbles may be produced in three ways.

1. For laminar flow of the gas through the orifice, as a bubble is detached from the orifice, the rupture and collapse of the elongated bubble neck may produce several very small bubbles. This tendency is markedly increased for solutions of low surface tension.
2. For turbulent flow of the gas through the orifice, bubbles of nonuniform size, including some very small bubbles, are produced by the shattering of large bubbles at a point approximately 3 to 4 in. above the orifice.
3. As turbulence is fully established for the flow of the gas through the orifice (at Reynolds numbers greater than 10,000), a progressively larger number of very small bubbles is torn away from the large irregular bubbles of the swirling discontinuous jet.

A limited number of data were obtained for the 1/64- and 1/32-in. orifices with entry of the air through the orifice-assembly tube pointed down at a 15-deg. angle with the horizontal. High-speed motion pictures and stroboscopic study of this mode of operation revealed that the jet of gas leaving the orifice is composed of discrete bubbles being ejected with a very rapid counterclockwise spiraling motion referred to an axis perpendicular to the plane of the orifice. The bubbles formed at the orifice are similar in shape to those formed at comparable flow rates with bottom entry. However, a gradation in bubble size is set up with respect to distance from the orifice. The largest bubbles (formed by the coalescence of smaller ones issuing from the orifice) rise from the jet at points very close to the orifice. The very fine bubbles formed by being torn off larger bubbles rise from the jet at the points farthest from the orifice. Bubbles of intermediate sizes rise from the jet at all points between these extremities. As the Reynolds number increases from 2,000 to 20,000, the dicontinuous jet of gas increases in length from approximately 1 to 6 in. With the present experimental apparatus, no data could be obtained for side entry with orifices greater than 1/32 in. in diameter, because the jet of gas collided with the wall of the experimental column for the larger orifices.

LAMINAR-FLOW RANGE

The bubbles are relatively uniform in size for the laminar flow of air through the orifice. As shown in Figures 1, 2, 3, 4, 10, and 11, very few minute bubbles are formed in the laminar-flow region. The frequency of bubble formation in this range was determined by stroboscopic examination. The mean bubble volume was calculated by use of the following equation:

$$v_B = \frac{q'}{f} \tag{1}$$

where v_B is the bubble volume, q' is the volumetric gas flow rate at the conditions of pressure and temperature downstream from the orifice, and f is the frequency of bubble formation. The average bubble diameter of a spherical bubble of equivalent bubble volume was calculated directly from average bubble volume obtained from Equation (1).

$$D_B = \left(\frac{6}{\pi} v_B\right)^{1/3} \tag{2}$$

Within the experimental error of this work, the volume and surface contributions of the small number of minute bubbles formed in the laminar-flow range may be considered negligible. Table 1 presents the results for bottom entrance flow as calculated from the stroboscopic studies of bubble formation from the 1/64-, 1/16-, and ⅛-in. orifices, respectively. The frequency of bubble formation is relatively constant (for a given orifice) and increases very slightly as the Reynolds number is increased. The calculated bubble diameter increases markedly as the Reynolds number is increased in the laminar-flow range. The data show that the bubble diameter varies as a function of orifice diameter in the laminar-flow range (i.e., constant-frequency region). For the air-water system, the following equation correlates the bubble diameter as a function of orifice diameter and Reynolds number:

$$D_B = 0.18 D_o^{1/2} N_{Re}^{1/3} \tag{3}$$

Davidson's results (*8*) for orifices ranging in diameter from approximately 0.04 to 0.40 in. may be expressed as

$$D_B = 0.19 D_o^{0.48} N_{Re}^{0.32} \tag{4}$$

The close agreement between Equations (3) and (4) is interesting. The orifice used by Davidson was drilled in the bottom flange of his experimental column. However, in this investigation, for bottom entrance flow, the orifice projected 12 in. into the column. Thus the presence of liquid in the column below the level of the orifice-assembly tube appears to have very little influence on the mechanics of bubble formation. The data are plotted as bubble diameter vs. Reynolds number on logarithmic coordinates in Figure 23. Since the bubbles are relatively uniform in size in the laminar-flow region, the calculated bubble diameters are equivalent to mean bubble diameters based on either the bubble volume, surface, or specific surface per unit volume (*6*).

BUBBLE-SIZE DISTRIBUTION*

Formation of nonuniform bubbles is initiated with the onset of turbulence for the gas flowing through the orifice. As turbulence becomes fully developed (i.e., $2{,}100 < N_{Re} < 10{,}000$), a randomization of bubble sizes occurs (Figures 5 to 9, 12 to 15, 19, and 20). To determine the effect of Reynolds number on D_{vs}, photographs were taken of a section of the column approximately 3 ft. above the orifice. The 4- by 5-in. negatives obtained were enlarged to 8- by 10-in. prints and the number of bubbles in the various size classes were determined visually by use of a pair of dividers and a scale. Figure 21 is a typical photograph employed to determine the bubble-diameter distribution. For the purposes of bubble-size measurements, it was assumed that all bubbles were located in a plane passing through the center line of the column. With the exception of very large bubbles, most of the bubbles were spherical in shape. The larger bubbles appeared to rise as oblate spheroids. However, oscillation in shape is noticeable in the motion of very large bubbles. The actual bubble sizes were determined by multiplying relative-scale sizes by a scale factor determined separately for each photograph.

The bubble-size-distribution data are fitted reasonably well by a logarithmic normal-probability distribution. The use of this function to correlate the data has a semitheoretical basis in that a repeated random process such as the breakup and coalescence of particles with growth or diminution by constant factors leads to a logarithmic probability distribution. In this investigation the smallest bubble size which could be measured by the photographic method employed is approximately 0.014 in. Consequently a truncated distribution was obtained, and it was necessary to fit a logarithmic normal-probability distribution to the data by an approximation method. The problem was to estimate the geometric mean and standard deviation for a logarithmic normally distributed population from a truncated sample in the case when neither frequencies nor measurements of variates in the omitted portion of the sample are known. Cohen (*4*) has developed a method of successive approximations whereby certain special functions required in the solutions of this problem given by Pearson and Lee (*22*) and Fisher (*10*) may be readily evaluated with the aid of an ordinary table of the areas and ordinates of the normal-probability curve (*20*).

The geometric mean for a logarithmic normal-probability distribution is defined by

$$\log D_G = \frac{\sum (n \log D_B)}{\sum n} \quad (5)$$

The standard deviation for a logarithmic normal-probability distribution is defined by

$$\sigma = \sqrt{\frac{\sum [n(\log D_B - \log D_G)^2]}{\sum n}} \quad (6)$$

The logarithmic probability function may be written

$$\varphi(z) = \frac{1}{\sqrt{2\pi}} e^{-z^2/2} \quad (7)$$

where z is defined by

$$z = \frac{\log D_B - \log D_G}{\sigma} \quad (8)$$

Data for a sample bubble-size distribution are plotted on logarithmic vs. cumulative probability coordinates in Figure 22. To determine the reproducibility of the distribution data, bubble-frequency counts were made on duplicate photographs for most of the points investigated. The logarithm of the geometric mean diameter and the standard deviation for the logarithmic normal probability distribution of best fit were obtained by Cohen's method (*4*). A Remington Rand analogue computer was employed to carry out the necessary calculations. The reproducibility of the data is shown to be reasonable. Several points, each representative of a single large bubble, show some scatter compared with the remainder of the data. The line plotted was drawn on the basis of the geometric mean and the standard deviation obtained from Cohen's method. The geometric mean is the bubble diameter corresponding to the value of 50% on the probability scale. The bubble diameters corresponding to the 84.13 and 15.87% sizes were obtained from the following:

$$\sigma = \frac{84.13\%\text{ size}}{50\%\text{ size}} = \frac{50\%\text{ size}}{15.87\%\text{ size}} \quad (9)$$

The total number of bubbles to be used in calculating the cumulative percentage greater than size from the frequency for each size range was obtained by an approximation method. By use of the line of best fit, the percentage greater than stated size was determined for each size range. The total number of bubbles was calculated from the frequency data for each size range as follows:

$$\sum n = \frac{n_1 + n_2 + \cdots + n_{\text{size}}}{\%\text{ greater than stated size}} \quad (10)$$

The abscissae of Figure 22 were based on the arithmetic average of the total numbers of bubbles obtained by use of the frequency data for each size range.

The standard deviation and the logarithm of the geometric mean bubble diameter for each of the bubble-size distributions obtained for the 1/64-, 1/32-, and 1/16-in. orifices with bottom entrance flow were used to calculate D_{vs}, the diameter of the bubble whose ratio of volume to surface area is equal to that of the entire bubble-size distribution (*6*). The following equation, developed by Hatch and Choate (*14*), was used to calculate D_{vs}.

$$\log D_{vs} = \log D_G + 5.757\sigma^2 \quad (11)$$

*Complete data on this section are filed as document 4958 with the American Documentation Institute, Photoduplication Service, Library of Congress, Washington 25, D. C., and may be obtained for $1.25 for photoprints or 35-mm. microfilm.

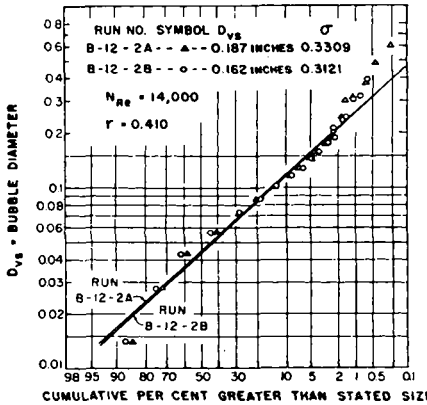

Fig. 22. Typical bubble-size distribution.

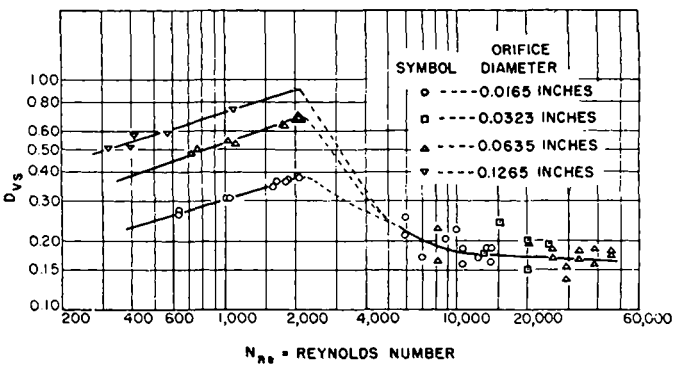

Fig. 23. Bottom-entrance-flow mean bubble diameter D_{vs} vs. Reynolds number.

TURBULENT-FLOW RANGE

The shattering of the large bubbles produced in turbulent flow with a resultant nonuniformity of bubble size has been discussed in a previous paragraph. The values of D_{vs} are plotted as a function of Reynolds number in Figure 23.

Only a very limited number of data are available for $2{,}100 < N_{Re} < 10{,}000$. With the onset of turbulence, the value of D_{vs} must be expected to drop very sharply, as shown by the dashed curves on Figure 23. This is reasonable, as the formation of very small bubbles is greatly increased as the discontinuous swirling jet is developed at the orifice. The data indicate that there is no noticeable effect of orifice diameter on D_{vs} in the turbulent-flow region. For the air-water system studied, the following equation fits the data for Reynolds numbers greater than 10,000:

$$D_{vs} = 0.28 N_{Re}^{-0.05} \qquad (12)$$

The data fit Equation (12) within the 95% confidence limits.

SUMMARY

Photographic studies of bubble formation reveal that nonuniformity of bubble size is initiated by the onset of turbulence in the air stream flowing through the orifice. In the section of the laminar-flow range studied in this investigation ($200 < N_{Re} < 2{,}100$) the frequency of bubble formation is nearly constant with respect to Reynolds number. The bubble size is relatively uniform at a given Reynolds number and depends markedly upon orifice diameter.

A normal distribution with respect to the logarithm of the bubble diameter is established for the turbulent flow of air through the orifice. As turbulence becomes fully developed, a marked decrease in D_{vs} occurs. For bottom entrance flow D_{vs} appears to be independent of the orifice diameter. The data indicate that a large increase of interfacial area may be effected in a gas-liquid contacting system by introducing the gas through orifices at Reynolds numbers greater than 10,000. The holdup of gas bubbles in a gas-liquid system was shown by Quigley (*23*) to be dependent on the 0.84 power of the gas rate of flow. Consequently, as the gas rate of flow is increased into the turbulent flow range, the resultant decrease in D_{vs} and the corresponding increase in gas holdup should greatly increase the gas-liquid interfacial contact area per unit volume.

It is important to note that the effects of liquid physical properties have not been studied in this investigation. The results obtained may be expected to apply qualitatively to similar systems. However, more data for bubble formation in other liquids (particularly of low surface tension) are necessary before a general correlation for bubble size in gas-liquid systems can be developed.

ACKNOWLEDGMENT

The authors wish to express their appreciation to S. T. Atkins, Jr., for his work in obtaining the photographs and motion pictures used in this investigation. The assistance of M. E. Ready and S. Chapman, E. Koval, and H. Cadolph in the statistical calculations involved in this study is gratefully acknowledged. The authors are indebted to G. B. Achorn, Jr., D. I. Dykstra, E. R. Dapper, and C. E. Cottrell, as well as many other staff members of Camp Detrick, for their suggestions and cooperation during the course of this study and to the U. S. Army Chemical Corps for permission to publish the paper.

NOTATION

		Dimension
A_o	= orifice cross-sectional area	L^2
c	= velocity of sound in the gas	L/θ
D_B	= bubble diameter	L
D_G	= geometric-mean bubble diameter	L
D_o	= orifice diameter	L
D_{vs}	= diameter of a bubble whose ratio of volume to surface is equivalent to that of the bubble-size distribution	L
f	= frequency of bubble formation	θ^{-1}
g_c	= conversion factor = 32.17 (lb./lb. force)(ft./sec.^{2})	$ML/F\theta^2$
n	= frequency of bubble-size class in bubble-size distribution	
N_{Re}	= Reynolds number = $4w/\pi D_o\mu$	
q	= volumetric rate of air flow at standard conditions 32°F. and 14.7 lb. force/sq. in.	L^3/θ
q'	= volumetric rate of air flow at the conditions of temperature and pressure downstream from the orifice	L^3/θ
r	= ratio of the absolute pressure downstream from the orifice to that upstream from the orifice	
V_B	= bubble volume	L^3
w	= mass rate of gas flow	M/θ
z	= logarithmic size variable, Equation (8)	
$\varphi(z)$	= probability function, Equation (7)	
ρ_g	= gas density	M/L^3
σ	= logarithmic standard deviation, Equation (6)	

LITERATURE CITED

1. Breitner, J. H., *Kolloid-Z.*, **100**, 335 (1942).
2. Castelman, R. A., *Natl. Advisory Comm. Aeronaut. Rept.* 440 (1932).
3. ———, *J. Research Natl. Bur. Standards*, **6**, 369 (1931).
4. Cohen, A. C., *J. Am. Statistical Assoc.*, **44**, 518 (1949).
5. Coppock, P. D., and G. T. Mieklejohn, *Trans. Inst. Chem. Engrs.*, **29**, 75 (1951).
6. DallaValle, J. M., "Micromeritics," Pitman Publishing Corp., New York (1948).
7. Datta, R. L., D. H. Napier, and D. M. Newitt, *Trans. Inst. Chem. Engrs.*, **28**, 14 (1950).
8. Davidson, L., Ph.D. thesis, Columbia Univ., New York (1951).
9. Eversole, W. G., G. H. Wagner, and E. Stackhouse, *Ind. Eng. Chem.*, **33**, 1459 (1941).
10. Fisher, R. A., "Mathematical Tables," Vol. 1, Brit. Soc. Advance. Sci. (1931).
11. Foulk, C. W., and J. N. Miller, *Ind. Eng. Chem.*, **23**, 1283 (1931).
12. Halberstadt, S., and P. H. Prausnitz, *Z. angew. Chem.*, **45**, 970 (1930).
13. Harkins, W. D., and F. E. Brown, *J. Am. Chem. Soc.*, **41**, 499 (1919).
14. Hatch, T., and S. P. Choate, *J. Franklin Inst.*, **207**, 369 (1929).
15. Hughes, R. R., A. E. Handlos, H. D. Evans, and R. L. Maycock, paper presented at the San Francisco meeting, Am. Inst. Chem. Engrs. (Sept. 14, 1953).
16. Jackson, R. W., *Ind. Chem.*, **28**, 346 (1952).
17. Jakob, Max, and W. Fritz, *Forsch. Gebiete Ingenieurw.*, **2**, 434 (1931).
18. Lee, A., *Biometrika*, **10**, 208 (1915).
19. Maier, C. G., *U. S. Bur. Mines Bull.* 260, 62 (1927).
20. Natl. Bur. Standards, "Tables of Normal Probability Functions," U. S. Govt. Printing Office, Washington, D. C. (1953).
21. Pattle, R. E., *Trans. Inst. Chem. Engrs.*, **28**, 32 (1950).
22. Pearson, K., and A. Lee, *Biometrika*, **6**, 59 (1908).
23. Quigley, C. J., *Chem. Eng. Progr., Symposium Series* No. 16, **51**, 31 (1955).
24. Schnurrmann, R., *Z. physik. Chem.*, **143A**, 456 (1929).
25. ———, *Kolloid-Z.*, **80**, 148 (1937).
26. *Ibid.*, **87**, 127 (1939).
27. Thomas, M. D., *Ind. Eng. Chem. (Anal. Ed.)*, **5**, 1939 (1935).
28. Turner, G. M., paper presented at the San Francisco meeting, Am. Inst. Chem. Engrs. (Sept. 14, 1953).
29. Van Krevelen, D. W., and P. J. Hoftijzer, *Chem. Eng. Progr.*, **46**, 29 (1950).
30. Verschoor, H. T., *Trans. Inst. Chem. Engrs.*, **28**, 52 (1950).
31. Wirth, H., *Arch. exp. Pathol. Pharmokol.*, **181**, 198 (1936).
32. Yamagata, K., F. Hirono, K. Nishikawa, and H. Matsuoka, *Japan Sci. Rev. Ser. II*, No. 4, 409 (1952).

Presented at A.I.Ch.E. Houston meeting